

Optimal Shape Design by Partial Spectral Data

Habib Ammari*

Yat Tin Chow†

Keji Liu‡

Jun Zou‡

Abstract

In this paper, we are concerned with a shape design problem, in which our target is to design, up to rigid transformations and scaling, the shape of an object given either its polarization tensor at multiple contrasts or the partial eigenvalues of its Neumann-Poincaré operator, which are known as the Fredholm eigenvalues. We begin by proposing to recover the eigenvalues of the Neumann-Poincaré operator from the polarization tensor by means of the holomorphic functional calculus. Then we develop a regularized Gauss-Newton optimization method for the shape reconstruction process. We present numerical results to demonstrate the effectiveness of the proposed methods and to illustrate important properties of the Fredholm eigenvalues and their associated eigenfunctions. Our results are expected to have important applications in the design of plasmon resonances in nanoparticles as well as in the multifrequency or pulsed imaging of small anomalies.

Mathematics Subject Classification (MSC 2000): 49J20, 47A75, 35R30, 35B30.

Keywords: optimal shape design, plasmonics, polarization tensor, Fredholm eigenvalues, Neumann-Poincaré operator, pulsed electrical capacitance tomography.

1 Introduction

Fredholm eigenvalues are the eigenvalues of the integral Neumann-Poincaré operator, which arises naturally in solving Neumann transmission problems for the Laplacian. They depend on the shape of the domain but they are invariant under rigid transformations and scaling. They have been the subject of intensive investigations; see, for instance, [1, 31, 32, 34]. Spectral analysis of Neumann-Poincaré type operators has played a key role in the mathematical justification of cloaking due to anomalous localized resonance [5] and in the analysis of gradient blow-up phenomena in the presence of nearly touching inclusions [6, 13, 14]. We also refer to [24] where new and interesting facts on spectral analysis related to the Neumann-Poincaré integral operator have been obtained and to the works on plasmon resonances [20, 27, 28]. Plasmon resonant nanoparticles such as gold nanoparticles offer, in addition to their biocompatibility, enhanced scattering and absorption, making them not only suitable for use as a contrast agent but also in therapeutic applications [20]. Recently, it has been shown that plasmon resonances in nanoparticles can be treated as an eigenvalue problem for the Neumann-Poincaré operator, which leads to direct calculation of resonance values of permittivity and resonance frequency [16, 28]. In biomedical applications, it is challenging to design nanoparticles that resonate at specified frequencies. It is the purpose of the paper to propose an efficient approach for solving the optimal design problem (up to rigid transformations and scaling) from partial Fredholm eigenvalues.

Shape identification from Fredholm eigenvalues has also important applications in imaging. In electrosensing, the polarization tensor (PT) of a target at multiple frequencies (or equivalently at multiple

*Department of Mathematics and Applications, Ecole Normale Supérieure, 45 Rue d'Ulm, 75005 Paris, France. The work of this author was supported by ERC Advanced Grant Project MULTIMOD-267184. (habib.ammari@ens.fr).

†Department of Mathematics, Chinese University of Hong Kong, Shatin, N.T., Hong Kong (ytchow@math.cuhk.edu.hk, kjliu@math.cuhk.edu.hk).

‡The work of this author was substantially supported by Hong Kong RGC grants (projects 405513 and 404611). (zou@math.cuhk.edu.hk)

contrasts) can be reconstructed from electrical capacitance measurements [2, 3, 4, 25, 33]. The PT arises naturally when we describe the perturbation of the electrical potential due to the presence of the target whose admittivity is different from that of the background. In fact, the polarization tensor of an inclusion can be expressed in terms of the Neumann-Poincaré operator and the admittivity contrast.

In this paper, we first show that the Fredholm eigenvalues can be reconstructed from the polarization tensor at multiple contrasts. By doing so, we connect design problems for plasmon resonances in nanoparticles to the imaging of small anomalies. Moreover, we show how to obtain in practice the polarization tensor at multiple contrasts from electrical capacitance tomography measurements. By probing the domain with an electric pulse, the polarization tensor of the anomaly at multiple frequencies and therefore at multiple contrasts can be recovered [18, 26]; see Appendix A. We optimize the pulse shape in order to reconstruct in the most stable way the first few Fredholm eigenvalues.

Then we consider the shape reconstruction problem (up to rigid transformations and scaling), in which we wish to reconstruct a shape from only the prior knowledge of the first several Fredholm eigenvalues of the Neumann-Poincaré operator. We start by giving both analytical and numerical evidence that the first Fredholm eigenvalues contain only low-frequency information about the shape of the domain while higher ones contain higher frequency information. We estimate the oscillation behavior of the associated eigenfunctions. We also emphasize the exponential decay of the Fredholm eigenvalues in the two dimensional case. This clearly makes the design problem exponentially ill-posed. Therefore, we should restrict ourselves to low-frequency shape reconstructions from the few first Fredholm eigenvalues.

We also derive Hadamard’s formula for the Fredholm eigenvalues. Based on Osborn’s theorem [29], we compute the shape derivative of Fredholm eigenvalues using the shape derivative of the Neumann-Poincaré operator. Then we propose a minimization algorithm to reconstruct a domain given its first Fredholm eigenvalues. In view of the invariance of the Fredholm eigenvalues under rigid transformations and scaling, we incorporate some effective penalty and regularization terms in the cost functional to ensure the local existence and uniqueness of its minimizers. We will further present several numerical illustrations of our main findings.

Our results on Fredholm eigenvalues and on the polarization tensor are expected to have important applications not only in shape design problems but also in shape classification and recognition problems. Various other geometric quantities associated with the shape of a domain, such as eigenvalues, capacities, harmonic moments, and generalized polarization tensors are used to distinguish between objects and classify them [3, 7, 8, 11, 12, 15, 19, 21]. The concept of polarization tensor at multiple contrasts seems to be the most natural one for shape classification and recognition using capacitance electrical impedance tomography.

The paper is organized as follows. In section 2, we introduce the Neumann-Poincaré operator and the concept of polarization tensor associated with a given domain and a given contrast. In section 3, two methods are provided for reconstructing Fredholm eigenvalues of a domain from its polarization tensor at all contrasts, then tested numerically. Section 4 is devoted to the derivation of a Hadamard’s perturbation formula for Fredholm eigenvalues. By combining the results in [11] on the shape derivative of the Neumann-Poincaré operator together with Osborn’s theorem [29], we compute the shape derivative of Fredholm eigenvalues. In section 5, we present and numerically test our minimization procedure for finding low-frequency features of a domain from its first few Fredholm eigenvalues. In Appendix A, we show the method to obtain the polarization tensors at multiple contrasts from electrical capacitance tomography measurements. In Appendix B, we consider the case of multiply connected objects. In that case, it is remarkable to easily find the number of connected components from the multiplicity of the Fredholm eigenvalues.

2 Neumann-Poincaré operator and polarization tensor

In this section, we first introduce the Neumann-Poincaré operator of an open connected domain D with \mathcal{C}^2 boundary in \mathbb{R}^d ($d = 2, 3$). Given such a domain D , we consider the following Neumann problem,

$$\Delta u = 0 \quad \text{in } D; \quad \frac{\partial u}{\partial \nu} = g \quad \text{on } \partial D, \quad \int_{\partial D} u \, d\sigma = 0, \quad (2.1)$$

where $g \in L_0^2(\partial D)$ with $L_0^2(\partial D)$ being the set of functions in $L^2(\partial D)$ with zero mean-value. In (2.1), $\partial/\partial \nu$ denotes the normal derivative. We note that the Neumann problem (2.1) can be rewritten as a boundary integral equation with the help of the single-layer potential. Given a density function $\phi \in L^2(\partial D)$, the single-layer potential, $\mathcal{S}_{\partial D}[\phi]$, can be defined as follows,

$$\mathcal{S}_{\partial D}[\phi](x) := \int_{\partial D} \Gamma(x-y)\phi(y)d\sigma(y) \quad (2.2)$$

for $x \in \mathbb{R}^d$, where Γ is the fundamental solution of the Laplacian in \mathbb{R}^d :

$$\Gamma(x-y) = \begin{cases} -\frac{1}{2\pi} \log |x-y| & \text{if } d=2, \\ \frac{1}{(2-d)\omega_d} |x-y|^{2-d} & \text{if } d>2, \end{cases} \quad (2.3)$$

where ω_d denotes the surface area of the unit sphere in \mathbb{R}^d . It is well-known that the single-layer potential satisfies the following jump condition on ∂D :

$$\frac{\partial}{\partial \nu} (\mathcal{S}_{\partial D}[\phi])^\pm = (\pm \frac{1}{2}I + \mathcal{K}_{\partial D}^*)[\phi], \quad (2.4)$$

where the superscripts \pm indicate the limits from outside and inside D respectively, and $\mathcal{K}_{\partial D}^* : L^2(\partial D) \rightarrow L^2(\partial D)$ is the Neumann-Poincaré operator defined by

$$\mathcal{K}_{\partial D}^*[\phi](x) := \frac{1}{\omega_d} \int_{\partial D} \frac{\langle x-y, \nu_x \rangle}{|x-y|^d} \phi(y) d\sigma(y), \quad (2.5)$$

with ν_x being the outward normal at $x \in \partial D$. We note that $\mathcal{K}_{\partial D}^*$ maps $L_0^2(\partial D)$ onto itself.

With these notions, the Neumann problem (2.1) can then be formulated as

$$g = \frac{\partial}{\partial \nu} (\mathcal{S}_{\partial D}[\phi])^- = (-\frac{1}{2}I + \mathcal{K}_{\partial D}^*)[\phi]. \quad (2.6)$$

Therefore, the solution to the Neumann problem (2.1) can be reformulated as a solution to the boundary integral equation with the Neumann-Poincaré operator $\mathcal{K}_{\partial D}^*$.

The operator $\mathcal{K}_{\partial D}^*$ arises not only in solving the Neumann problem for the Laplacian but also for representing the solution to the transmission problem as described below.

Consider an open connected domain D with \mathcal{C}^2 boundary in \mathbb{R}^d . Given a harmonic function u_0 in \mathbb{R}^d , we consider the following transmission problem in \mathbb{R}^d :

$$\begin{cases} \nabla \cdot (\varepsilon_D \nabla u) = 0 & \text{in } \mathbb{R}^d, \\ u - u_0 = O(|x|^{1-d}) & \text{as } |x| \rightarrow \infty, \end{cases} \quad (2.7)$$

where $\varepsilon_D = \varepsilon_c \chi(D) + \varepsilon_m \chi(\mathbb{R}^d \setminus \overline{D})$ with $\varepsilon_c, \varepsilon_m$ being two positive constants, and $\chi(\Omega)$ is the characteristic function of the domain $\Omega = D$ or $\mathbb{R}^d \setminus \overline{D}$. With the help of the single-layer potential, we can rewrite the perturbation $u - u_0$, which is due to the inclusion D , as

$$u - u_0 = \mathcal{S}_{\partial D}[\phi], \quad (2.8)$$

where $\phi \in L^2(\partial D)$ is an unknown density, and $\mathcal{S}_{\partial D}[\phi]$ is the refraction part of the potential in the presence of the inclusion. The transmission problem (2.7) can be rewritten as

$$\begin{cases} \Delta u = 0 & \text{in } D \cup (\mathbb{R}^d \setminus \overline{D}), \\ u^+ = u^- & \text{on } \partial D, \\ \varepsilon_c \frac{\partial u^+}{\partial \nu} = \varepsilon_m \frac{\partial u^-}{\partial \nu} & \text{on } \partial D, \\ u - u_0 = O(|x|^{1-d}) & \text{as } |x| \rightarrow \infty. \end{cases} \quad (2.9)$$

With the help of the jump condition (2.4), solving the above system (2.9) can be regarded as solving the density function $\phi \in L^2(\partial D)$ of the following integral equation

$$\frac{\partial u_0}{\partial \nu} = \left(\frac{\varepsilon_c + \varepsilon_m}{2(\varepsilon_c - \varepsilon_m)} I - \mathcal{K}_{\partial D}^* \right) [\phi]. \quad (2.10)$$

With the harmonic property of u_0 , we can write

$$u_0(x) = \sum_{\alpha \in \mathbb{N}^d} \frac{1}{\alpha!} \partial^\alpha u_0(0) x^\alpha \quad (2.11)$$

with $\alpha = (\alpha_1, \dots, \alpha_d) \in \mathbb{N}^d$, $\partial_\alpha = \partial_1^{\alpha_1} \dots \partial_d^{\alpha_d}$ and $\alpha! = \alpha_1! \dots \alpha_d!$.

Consider ϕ^α as the solution of the Neumann-Poincaré operator:

$$\frac{\partial x^\alpha}{\partial \nu} = \left(\frac{\varepsilon_c + \varepsilon_m}{2(\varepsilon_c - \varepsilon_m)} I - \mathcal{K}_{\partial D}^* \right) [\phi^\alpha]. \quad (2.12)$$

The invertibilities of the operator $(\frac{\varepsilon_c + \varepsilon_m}{2(\varepsilon_c - \varepsilon_m)} I - \mathcal{K}_{\partial D}^*)$ from $L^2(\partial D)$ onto $L^2(\partial D)$ and from $L_0^2(\partial D)$ onto $L_0^2(\partial D)$ are proved, for example, in [9, 23], provided that $|\frac{\varepsilon_c + \varepsilon_m}{2(\varepsilon_c - \varepsilon_m)}| > 1/2$. We can substitute (2.11) and (2.12) back into (2.8) to get

$$u - u_0 = \sum_{|\alpha| \geq 1} \frac{1}{\alpha!} \partial^\alpha u_0(0) \mathcal{S}_{\partial D}[\phi^\alpha] = \sum_{|\alpha| \geq 1} \frac{1}{\alpha!} \partial^\alpha u_0(0) \int_{\partial D} \Gamma(x - y) \phi^\alpha(y) d\sigma(y). \quad (2.13)$$

Using the Taylor expansion,

$$\Gamma(x - y) = \Gamma(x) - y \cdot \nabla \Gamma(x) + O\left(\frac{1}{|x|^d}\right), \quad (2.14)$$

which holds for all x such that $|x| \rightarrow \infty$ while y is bounded [9], we get the following result by substituting (2.14) into (2.13) that

$$(u - u_0)(x) = \nabla u_0(0) \cdot M(\lambda, D) \nabla \Gamma(x) + O\left(\frac{1}{|x|^d}\right) \quad \text{as } |x| \rightarrow \infty, \quad (2.15)$$

where $M = (m_{ij})_{i,j=1}^d$ is the polarization tensor (PT) associated with the domain D and the contrast λ defined by

$$m_{ij}(\lambda, D) := \int_{\partial D} y_i (\lambda I - \mathcal{K}_{\partial D}^*)^{-1} [\nu_j](y) d\sigma(y), \quad (2.16)$$

with $\lambda := \frac{\varepsilon_c + \varepsilon_m}{2(\varepsilon_c - \varepsilon_m)}$ and ν_j being the j -th component of ν . Here we have used in (2.15) the fact that $\int_{\partial D} \nu d\sigma = 0$.

Typically the constants ε_c and ε_m are positive in order to make the system (2.9) physical. This corresponds to the situation with $|\lambda| > \frac{1}{2}$.

However, recent advances in nanotechnology make it possible to produce noble metal nanoparticles with negative permittivities at optical frequencies [20, 30]. Therefore, we can have the possibility for some frequencies that $\lambda := \frac{\varepsilon_c + \varepsilon_m}{2(\varepsilon_c - \varepsilon_m)}$ actually lies in the spectrum of $\mathcal{K}_{\partial D}^*$.

If this happens, the following integral equation

$$0 = (\lambda I - \mathcal{K}_{\partial D}^*)[\phi] \quad \text{on } \partial D \quad (2.17)$$

has non-trivial solutions $\phi \in L^2(\partial D)$ and the nanoparticle resonates at those frequencies.

Therefore, we have to investigate the mapping properties of the Neumann-Poincaré operator. Assume that ∂D is of class $\mathcal{C}^{1,\alpha}$. It is known that the operator $\mathcal{K}_{\partial D}^* : L^2(\partial D) \rightarrow L^2(\partial D)$ is compact [23], and its spectrum is discrete and accumulates at zero. All the eigenvalues are real and bounded by $1/2$. Moreover, $1/2$ is always an eigenvalue and its associated eigenspace is of dimension one, which is nothing else but the kernel of the single-layer potential $\mathcal{S}_{\partial D}$. In two dimensions, it can be proved that if $\lambda_i \neq 1/2$ is an eigenvalue of $\mathcal{K}_{\partial D}^*$, then $-\lambda_i$ is an eigenvalue as well. This property is known as the twin spectrum property; see [27]. The Fredholm eigenvalues are the eigenvalues of $\mathcal{K}_{\partial D}^*$. It is easy to see, from the properties of $\mathcal{K}_{\partial D}^*$, that they are invariant with respect to rigid motions and scaling. They can be explicitly computed for ellipses and spheres. If a and b denote the semi-axis lengths of an ellipse then it can be shown that $\pm(\frac{a-b}{a+b})^i$ are its Fredholm eigenvalues [24]. For the sphere, they are given by $1/(2(2i+1))$; see [22]. It is worth noticing that the convergence to zero of Fredholm eigenvalues is exponential for ellipses while it is algebraic for spheres.

Equation (2.17) corresponds to the case when plasmonic resonance occurs in D ; see [16]. The optimal shape design for Fredholm eigenvalues is of great interest in plasmonics [20, 27, 30]. Given negative values of ε_c , we show in this paper how to design a shape with prescribed plasmonic resonances.

3 Reconstruction of Fredholm eigenvalues from the polarization tensor

3.1 Reconstruction method via holomorphic functional calculus

In this subsection we propose for two dimensions to recover the Fredholm eigenvalues from the polarization tensor

$$M(\lambda, D) := \int_{\partial D} y(\lambda I - \mathcal{K}_{\partial D}^*)^{-1}[\nu](y) d\sigma(y) \quad (3.1)$$

for λ along a simple closed curve γ by means of the holomorphic functional calculus. From this expression, one observes that $M(\lambda, D)$ actually encodes vast information of the resolvent of the operator $\mathcal{K}_{\partial D}^*$ at λ ,

$$R_\lambda(\mathcal{K}_{\partial D}^*) := (\lambda I - \mathcal{K}_{\partial D}^*)^{-1}. \quad (3.2)$$

Motivated by this observation, we propose to recover eigenvalues $\{\lambda_i\}_{i \geq 1}$ ($\lambda_i \neq 1/2$) of $\mathcal{K}_{\partial D}^*$ from $M(\lambda, D)$ via the holomorphic functional calculus of $\mathcal{K}_{\partial D}^*$. Let \mathcal{H} be the space $L_0^2(\partial D)$ equipped with the inner product $-\langle \cdot, \mathcal{S}_{\partial D}(\cdot) \rangle_{L^2(\partial D)}$. Since $\mathcal{S}_{\partial D}$ is injective on $L_0^2(\partial D)$, $L_0^2(\partial D)$ is complete for this inner product. If ∂D is of class $\mathcal{C}^{1,\alpha}$, there exists a complete orthonormal set $\{\phi_i^\pm\}_{i \geq 1}$ in \mathcal{H} such that $\mathcal{K}_{\partial D}^* \phi_i^\pm = \pm \lambda_i \phi_i^\pm$ for all $i \geq 1$ and the eigenvalues $1/2 > \lambda_1 \geq \dots \geq \lambda_i \rightarrow 0$ as $i \rightarrow \infty$, by using the self-adjointness and the compactness of the operator $\mathcal{K}_{\partial D}^*$ over \mathcal{H} and the Hilbert-Schmidt theorem; see [24]. For notational sake, we will often write $\lambda_i^\pm := \pm \lambda_i$ in our subsequent discussions. Then we can decompose the operator $\mathcal{K}_{\partial D}^*$ as

$$\mathcal{K}_{\partial D}^* = \sum_{i=1}^{\infty} \left\{ \lambda_i^+ \langle \phi_i^+, \cdot \rangle_{\mathcal{H}} \phi_i^+ + \lambda_i^- \langle \phi_i^-, \cdot \rangle_{\mathcal{H}} \phi_i^- \right\} = \sum_{i=1}^{\infty} \lambda_i \left\{ \langle \phi_i^+, \cdot \rangle_{\mathcal{H}} \phi_i^+ - \langle \phi_i^-, \cdot \rangle_{\mathcal{H}} \phi_i^- \right\}. \quad (3.3)$$

Note that as $\mathcal{K}_{\partial D}^*$ is a pseudo-differential operator of order -1 , the eigenfunctions ϕ_i^\pm oscillate as $1/\lambda_i$, and there exists a positive constant C such that

$$\frac{\|\frac{\partial \phi_i^\pm}{\partial T}\|_{L^2(\partial D)}}{\|\phi_i^\pm\|_{L^2(\partial D)}} \lesssim \frac{C}{\lambda_i},$$

where $\partial/\partial T$ denotes the tangential derivative.

Now, given the Neumann-Poincaré operator $\mathcal{K}_{\partial D}^*$ corresponding to a shape D (D being an open domain with $\mathcal{C}^{1,\alpha}$ boundary), we define, for any holomorphic function f on an open domain $U \subset \mathbb{C}$ containing the spectrum of $\mathcal{K}_{\partial D}^*$, the following notion

$$f(\mathcal{K}_{\partial D}^*) := \sum_{i=1}^{\infty} \left[f(\lambda_i^+) \langle \phi_i^+, \cdot \rangle_{\mathcal{H}} \phi_i^+ + f(\lambda_i^-) \langle \phi_i^-, \cdot \rangle_{\mathcal{H}} \phi_i^- \right]. \quad (3.4)$$

Clearly, if f is a polynomial in $z \in \mathbb{C}$, say $f(z) := \sum_{i=0}^N a_i z^i$ for some $N \in \mathbb{N}$, the definition (3.4) coincides with the conventional one, i.e., $f(\mathcal{K}_{\partial D}^*) = \sum_{i=0}^N a_i (\mathcal{K}_{\partial D}^*)^i$, where $(\mathcal{K}_{\partial D}^*)^i$ means the composition of the operator i times. For our subsequent description, we may write for any $\phi \in L^2(\partial D)$ that

$$\langle \phi, y \rangle_{L^2(\partial D)} := \int_{\partial D} y \phi(y) d\sigma(y).$$

Then we have the following representation result.

Lemma 3.1. *Given a shape D and the corresponding Neumann-Poincaré operator $\mathcal{K}_{\partial D}^*$, the following identity holds for the polarization tensor $M(\lambda, D)$ in (3.1) and any holomorphic function f on an open domain $U \subset \mathbb{C}$ containing the spectrum $\sigma(\mathcal{K}_{\partial D}^*)$ of $\mathcal{K}_{\partial D}^*$:*

$$\frac{1}{2\pi i} \int_{\gamma} f(\lambda) M(\lambda, \partial D) d\lambda = \int_{\partial D} y f(\mathcal{K}_{\partial D}^*) [\nu](y) d\sigma(y) = \sum_{i=1}^{\infty} \left[c_i^+ f(\lambda_i^+) + c_i^- f(\lambda_i^-) \right], \quad (3.5)$$

where γ is an arbitrary simple closed curve in U enclosing $\sigma(\mathcal{K}_{\partial D}^*)$, and c_i^+ and c_i^- are defined by

$$c_i^+ := \langle \nu, \phi_i^+ \rangle_{\mathcal{H}} \langle \phi_i^+, y \rangle_{L^2(\partial D)}, \quad c_i^- := \langle \nu, \phi_i^- \rangle_{\mathcal{H}} \langle \phi_i^-, y \rangle_{L^2(\partial D)}. \quad (3.6)$$

Proof. By the holomorphic functional calculus, we know for any holomorphic function f on an open domain $U \subset \mathbb{C}$ containing $\sigma(\mathcal{K}_{\partial D}^*)$ and any simple closed curve γ in U enclosing $\sigma(\mathcal{K}_{\partial D}^*)$ that

$$\frac{1}{2\pi i} \int_{\gamma} f(\lambda) R_{\lambda}(\mathcal{K}_{\partial D}^*) d\lambda = f(\mathcal{K}_{\partial D}^*) = \sum_{i=1}^{\infty} \left[f(\lambda_i^+) \langle \phi_i^+, \cdot \rangle_{\mathcal{H}} \phi_i^+ + f(\lambda_i^-) \langle \phi_i^-, \cdot \rangle_{\mathcal{H}} \phi_i^- \right]. \quad (3.7)$$

Combining this with (3.1), we readily derive that

$$\frac{1}{2\pi i} \int_{\gamma} f(\lambda) M(\lambda, \partial D) d\lambda = \int_{\partial D} y f(\mathcal{K}_{\partial D}^*) [\nu](y) d\sigma(y). \quad (3.8)$$

Now the desired representation comes from the above two identities. \square

We note that even if ∂D is only Lipschitz, a similar result can be obtained for the (noncompact) operator $\mathcal{K}_{\partial D}^*$ from the spectral decomposition $\mathcal{K}_{\partial D}^* = \int \lambda dE_{\lambda}$ where E_{λ} is the projection-valued measure. However, we will not pursue in this direction for the sake of simplicity. We refer the reader to [17].

Based on the relation (3.5), we can make use of different choices of holomorphic functions f to reconstruct the eigenvalues λ_i of $\mathcal{K}_{\partial D}^*$ from its polarization tensor. One of the methods is based on the following observation. For any $n \in \mathbb{N}$ we define

$$h_1^{(n)} := \frac{1}{2\pi i} \int_{\gamma} \lambda^{2n} M(\lambda, \partial D) d\lambda, \quad (3.9)$$

$$h_j^{(n)} := \frac{1}{2\pi i} \int_{\gamma} \lambda^{2n} M(\lambda, \partial D) d\lambda - \sum_{i=1}^{j-1} (c_i^+ + c_i^-) \lambda_i^{2n} \quad \text{for } j > 1, \quad (3.10)$$

then we come to the following corollary.

Corollary 3.2. *Assume that all the eigenvalues of $\mathcal{K}_{\partial D}^*$ are simple. Then for any $j \in \mathbb{N}$ such that $c_j^+ + c_j^- \neq 0$, it holds that*

$$\lim_{n \rightarrow \infty} \frac{h_j^{(n)}}{h_j^{(n-1)}} = \lambda_j^2 \quad \text{and} \quad \lim_{n \rightarrow \infty} \frac{h_j^{(n)}}{\lambda_j^{2n}} = c_i^+ + c_i^-. \quad (3.11)$$

Proof. Taking $f = \lambda^{2n}$ for $n \in \mathbb{N}$ in (3.5), we have

$$\frac{1}{2\pi i} \int_{\gamma} \lambda^{2n} M(\lambda, \partial D) d\lambda = \sum_{i=1}^{\infty} \left[c_i^+ (\lambda_i)^{2n} + c_i^- (-\lambda_i)^{2n} \right] = \sum_{i=1}^{\infty} (c_i^+ + c_i^-) \lambda_i^{2n}. \quad (3.12)$$

Substituting (3.12) into (3.9)-(3.10), we get that for all $j \in \mathbb{N}$,

$$h_j^{(n)} = \sum_{i=j}^{\infty} (c_i^+ + c_i^-) \lambda_i^{2n}. \quad (3.13)$$

Noting that all the eigenvalues of $\mathcal{K}_{\partial D}^*$ are simple and $c_j^+ + c_j^- \neq 0$, we readily obtain from (3.13) that

$$\lim_{n \rightarrow \infty} \frac{h_j^{(n)}}{h_j^{(n-1)}} = \lim_{n \rightarrow \infty} \frac{\sum_{i=j}^{\infty} (c_i^+ + c_i^-) \lambda_i^{2n}}{\sum_{i=j}^{\infty} (c_i^+ + c_i^-) \lambda_i^{2(n-1)}} = \lambda_j^2, \quad (3.14)$$

and

$$\lim_{n \rightarrow \infty} \frac{h_j^{(n)}}{\lambda_j^{2n}} = \lim_{n \rightarrow \infty} \sum_{i=j}^{\infty} (c_i^+ + c_i^-) \left(\frac{\lambda_i}{\lambda_j} \right)^{2n} = c_j^+ + c_j^-. \quad (3.15)$$

This gives the conclusion of the corollary. \square

With the help of Corollary 3.2, we can propose the following method to reconstruct the Fredholm eigenvalues from the polarization tensor at multiple contrasts.

Method 1. Given two integers $J, N \in \mathbb{N}$. For $j = 1, 2, \dots, J$ and $n = 1, 2, \dots, N$, compute $h_j^{(n)}$ based on (3.9)-(3.10), then compute the square root of the quotient

$$\sqrt{h_j^{(n)} / h_j^{(n-1)}}$$

for the approximation of the eigenvalue λ_j .

Next, we introduce another reconstruction method. For a $\sigma_0 > 0$, $t \in \mathbb{R}$ and a simple closed curve γ enclosing $\sigma(\mathcal{K}_{\partial D}^*)$, we define

$$\Phi_{\sigma_0, \gamma}(t) := \frac{1}{2\pi i} \int_{\gamma} \exp\left(-\frac{(\lambda - t)^2}{2\sigma_0^2}\right) M(\lambda, \partial D) d\lambda. \quad (3.16)$$

Then by taking a different holomorphic function f in (3.5), we have the following useful result from Lemma 3.1.

Corollary 3.3. *Given a shape D and the corresponding Neumann-Poincaré operator $\mathcal{K}_{\partial D}^*$, the following equality holds*

$$\Phi_{\sigma_0, \gamma}(t) = \sum_{i=1}^{\infty} \left[c_i^+ \exp\left(-\frac{(\lambda_i - t)^2}{2\sigma_0^2}\right) + c_i^- \exp\left(-\frac{(\lambda_i + t)^2}{2\sigma_0^2}\right) \right]. \quad (3.17)$$

Proof. For $\sigma_0 > 0$ and $t \in \mathbb{R}$, let $f(\lambda, t) := \exp(-\frac{(\lambda-t)^2}{2\sigma_0^2})$. As $f(\lambda, t)$ is holomorphic with respect to λ , we can substitute it in (3.5) to get the desired representation. \square

Noting that the function $\exp(-\frac{(\lambda_i-t)^2}{2\sigma_0^2})$ achieves its maximum at $t = \lambda_i$ and decays exponentially away from $t = \lambda_i$, we observe from (3.17) that the local extrema of the function $\Phi_{\sigma_0, \gamma}(t)$ are approximately located at the eigenvalues λ_i of operator $\mathcal{K}_{\partial D}^*$. So we can reconstruct the eigenvalues λ_i by evaluating the local extrema of function $\Phi_{\sigma_0, \gamma}(t)$. This leads us to the following second reconstruction method.

Method 2. Given a small constant $\sigma_0 > 0$. Evaluate function $\Phi_{\sigma_0, \gamma}(t)$ in (3.16) for $t \in [-1/2, 1/2]$. Then locate the local extrema of function $\Phi_{\sigma_0, \gamma}(t)$ one by one, starting from the one with the largest magnitude of c_i^\pm , then moving to the one with the second largest magnitude of c_i^\pm , and so on.

3.2 Numerical results

In this subsection, we will first present some numerical results on the approximations of the Fredholm eigenvalues and the decay properties of eigenvalues. Then we shall focus on the inverse problem to reconstruct the Fredholm eigenvalues from the observed PT at multiple contrasts.

For the approximations of the Neumann-Poincaré operator and Fredholm eigenvalues, we use a fine mesh of size $h = 1/1024$ to discretize the integral operator (2.5) by the trapezoidal quadrature rule over the curve ∂D , and compute the eigenvalues of $\mathcal{K}_{\partial D}^*$.

For a given shape D , we plot the decay of eigenvalues and the growth of oscillation. Let λ_i be the i -th eigenvalue and ϕ_i^+ be the corresponding eigenfunction. Then we define the oscillation of the eigenfunction ϕ_i^+ by

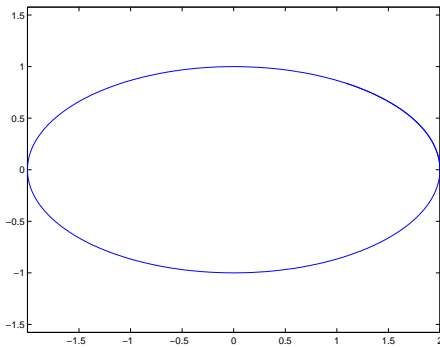
$$a_i := \frac{\|\frac{\partial \phi_i^+}{\partial T}\|_{L^2(\partial D)}}{\|\phi_i^+\|_{L^2(\partial D)}}, \quad i \geq 1. \quad (3.18)$$

In Figures 1 and 2, we can see the detailed changes of λ_i against i , $\log \lambda_i$ against i , and a_i against i , from which one can observe the decay of eigenvalues and the growth of oscillation of eigenfunctions, corresponding to two domains D , an ellipse of the form

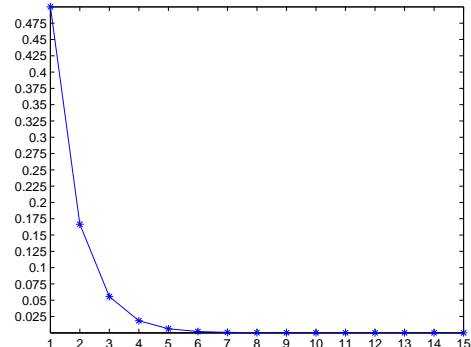
$$\frac{x^2}{4} + y^2 = 1, \quad x, y \in \mathbb{R}, \quad (3.19)$$

and a heart-shaped domain of the form (with $\delta = 0.8$ and $m = 1$):

$$r = 1 + \delta \sin(m\theta), \quad \theta \in (0, 2\pi]. \quad (3.20)$$



(a)



(b)

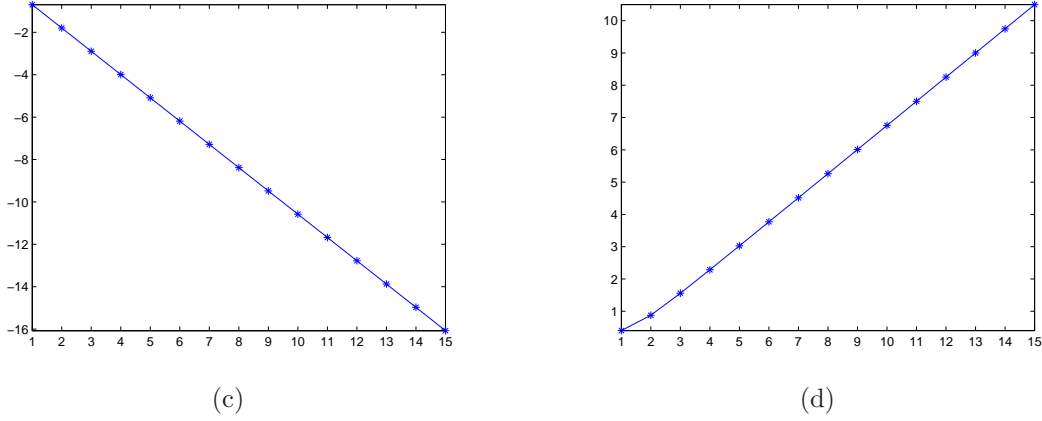


Figure 1: (a) Domain D ; (b) λ_i against i ; (c) $\log \lambda_i$ against i ; (d) a_i against i .

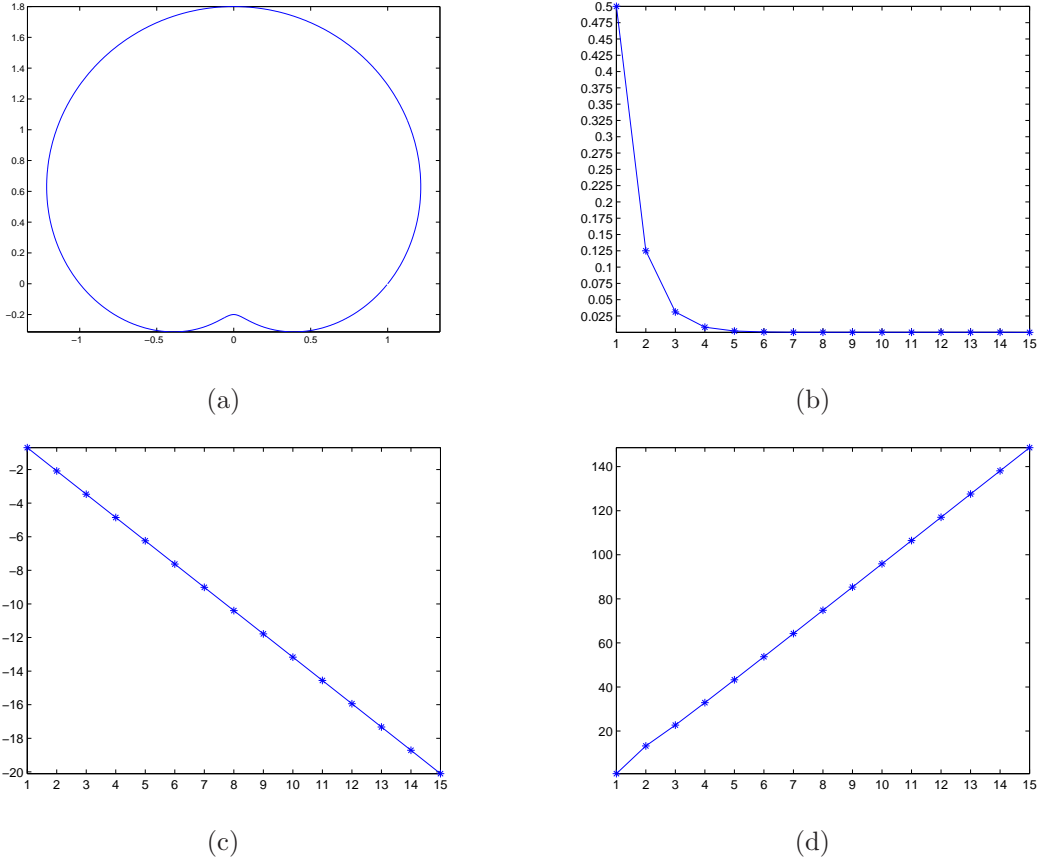


Figure 2: (a) Domain D ; (b) λ_i against i ; (c) $\log \lambda_i$ against i ; (d) a_i against i .

Next, we carry out some numerical examples for the reconstructions of Fredholm eigenvalues from PT at multiple contrasts. The forward data is obtained by first approximating the Neumann-Poincaré operator as it was done earlier in this subsection, then the PT, $M(\lambda, D) = (m_{ij}(\lambda, D))_{i,j=1}^d$, is calculated based on (3.1) using the trapezoidal rule over a fine mesh of size $h = 1/1024$ on ∂D . Values of $M(\lambda, D)$ are obtained for $\lambda \in \mathbb{C}$ on the grid points of a uniform mesh of size $1/100$ over the curve γ :

$$\gamma = \{0.23 e^{2\pi i \theta} + 0.3 \mid 0 \leq \theta \leq 1\}, \quad (3.21)$$

and are regarded as the observed data for the reconstructions of the Fredholm eigenvalues. For the numerical comparisons, we have implemented both Methods 1 and 2 in Section 3.1. We notice that, in Method 1, quadrature rules with accuracy of very higher orders are necessary for the approximation of the contour integration in order to accurately approximate $h_1^{(n)}$ in (3.9) for large $n \in \mathbb{N}$, which is the case for an accurate estimate of eigenvalues. Hence Method 1 may be rather expensive, and we shall demonstrate only the reconstructions by Method 2 below.

By considering only those eigenvalues lying inside γ (which are all positive), we compute (3.16) in our implementations of Method 2 as follows:

$$\Phi_{\sigma_0, \gamma}(t) := \frac{1}{2\pi i} \int_{\gamma} \exp\left(-\frac{(\lambda - t)^2}{2\sigma_0^2}\right) M(\lambda, \partial D) d\lambda = \sum_{0.07 < \lambda_i < 0.53} c_i^+ \exp\left(-\frac{(\lambda_i - t)^2}{2\sigma_0^2}\right) \quad (3.22)$$

with $\sigma_0 = 0.05$. Then we can locate the local extrema of function (3.22) one by one, starting from the one with the largest magnitude of c_i^+ , then to the one with the second largest magnitude of c_i^+ , and so on. This process provides us with a set of approximate eigenvalues from the knowledge of polarization tensor $M(\lambda, \partial D)$ over γ . The exact eigenvalues and the approximate ones obtained from the above described Method 2 are listed in Table 1 for the kite-shaped domain D of the form

$$x = \cos \theta + 0.65 \cos 2\theta - 0.65, \quad y = 1.5 \sin \theta, \quad \theta \in (0, 2\pi], \quad (3.23)$$

a pear-shaped domain in Table 2 and a floriform domain with 3 petals in Table 3. Here the latter two domains are of the form (3.20) with the same parameter $m = 3$ but a different δ , i.e., $\delta = 0.3$ and 0.6 .

Eigenvalues	Exact solutions	Approximate solutions
First	0.5000	0.5000
Second	0.2707	0.2700
Third	0.1902	0.1800
Fourth	0.0891	0.0900
Fifth	0.0718	0.0700

Table 1: *The first 5 reconstructed eigenvalues for the kite-shaped domain.*

Eigenvalues	Exact solutions	Approximate solutions
First	0.5000	0.5000
Second	0.1035	0.1050
Third	0.1035	0.1050

Table 2: *The first 3 reconstructed eigenvalues for the pear-shaped domain.*

Eigenvalues	Exact solutions	Approximate solutions
First	0.5000	0.5000
Second	0.3322	0.3300
Third	0.3322	0.3300
Fourth	0.1404	0.1300
fifth	0.1404	0.1300

Table 3: *The first 5 reconstructed eigenvalues for the floriform domain.*

As we can observe from Tables 1, 2 and 3, the reconstructed eigenvalues are rather satisfactory and accurate in view of the severe ill-posedness of recovering eigenvalues.

4 Hadamard's formula for the Fredholm eigenvalues

In this section, we turn our attention to the optimal shape design problem given the Fredholm eigenvalues corresponding to a geometric shape. Our tactic to approach the problem is via an optimization

of a least-squares functional. For this purpose, we first discuss how to obtain the shape derivatives of the Neumann-Poincaré operator and the Fredholm eigenvalues. These derivatives are needed when we compute the gradient of least-squares functional concerned.

To start with, we first focus on the shape derivative of the Neumann-Poincaré operator, which was derived in [11]. We need some new notations for the description of derivative. Given a shape D and $a, b \in \mathbb{R}$ with $a < b$, we consider an arc-length parametrization of ∂D , $X(t) : [a, b] \rightarrow \partial D$. Let $T(x)$ and $\nu(x)$ be respectively the tangent vector and the outward unit normal to ∂D at $x \in \partial D$, and $\tau(x)$ be the curvature defined by

$$X''(t) = \tau(x)\nu(x). \quad (4.1)$$

Now consider an ε -perturbation of D , namely ∂D_ε is given by

$$\partial D_\varepsilon := \{\tilde{x} \mid \tilde{x} = x + \varepsilon h(x)\nu(x), x \in \partial D\}, \quad (4.2)$$

where $h \in C^1(\partial D)$. For two arbitrary points $x, y \in \partial D$ such that $x = X(t), y = X(s)$ for some $t, s \in [a, b]$, we define

$$F_h(x, y) = \frac{\langle x - y, h(t)x(x) - h(s)\nu(y) \rangle}{|x - y|^2} \quad \text{and} \quad G_h(x, y) = \frac{|h(t)x(x) - h(s)\nu(y)|^2}{|x - y|^2}, \quad (4.3)$$

and $F_{h,n}$ as the coefficients in the following series

$$\sum_{n=0}^{\infty} \varepsilon^n F_{h,n}(x, y) := \frac{1}{1 + 2\varepsilon F_h(x, y) + \varepsilon^2 G_h(x, y)} \frac{\sqrt{(1 - \varepsilon \tau(y)h(s))^2 + \varepsilon^2 (h'(s))^2}}{\sqrt{(1 - \varepsilon \tau(x)h(t))^2 + \varepsilon^2 (h'(t))^2}}, \quad (4.4)$$

where the series converges absolutely and uniformly [11]. We can directly see that

$$F_{h,0}(x, y) = 0 \quad \text{and} \quad F_{h,1}(x, y) = -2F_h(x, y) + \tau(x)h(x) - \tau(y)h(y). \quad (4.5)$$

For any two points $\tilde{x}, \tilde{y} \in \partial D_\varepsilon$ such that $\tilde{x} := x + \varepsilon h(t)\nu(x)$ and $\tilde{y} := y + \varepsilon h(s)\nu(y)$, we write $\mathbb{K}_{h,n}$ as the coefficients in the following series

$$\sum_{n=0}^{\infty} \varepsilon^n \mathbb{K}_{h,n}(x, y) d\sigma(y) := \frac{\langle \tilde{x} - \tilde{y}, \tilde{\nu}(\tilde{x}) \rangle}{|\tilde{x} - \tilde{y}|^2} d\sigma_\varepsilon(\tilde{y}), \quad (4.6)$$

where $\tilde{\nu}(\tilde{x})$ denotes the outward unit normal to ∂D_ε at \tilde{x} , while $d\sigma(y)$ and $d\sigma_\varepsilon(\tilde{y})$ are the length elements on ∂D at y and on ∂D_ε at \tilde{y} respectively. Then, following the argument in [11] and using (4.3)-(4.4) and (4.6) we have

$$\mathbb{K}_{h,0} = \frac{\langle x - y, \nu(x) \rangle}{|x - y|^2}, \quad \mathbb{K}_{h,1} = K_{h,0}F_{h,1} + K_{h,1}, \quad \mathbb{K}_{h,n} = F_{h,n}K_{h,0} + F_{h,n-1}K_{h,1} + F_{h,n-2}K_{h,2},$$

for $n \geq 2$, where $K_{h,0}$, $K_{h,1}$ and $K_{h,2}$ are given by

$$\begin{aligned} K_{h,0} &= \frac{\langle x - y, \nu(x) \rangle}{|x - y|^2}, \\ K_{h,1} &= \frac{\langle h(t)\nu(x) - h(s)\nu(y), \nu(x) \rangle}{|x - y|^2} - \frac{\langle x - y, \tau(x)h(t)\nu(x) + h'(t)T(x) \rangle}{|x - y|^2}, \\ K_{h,2} &= \frac{\langle h(t)\nu(x) - h(s)\nu(y), \tau(x)h(t)\nu(x) - h'(t)T(x) \rangle}{|x - y|^2}. \end{aligned}$$

Define a sequence of integral operators $\mathcal{K}_{D,h}^{(n)} : L^2(\partial D) \rightarrow L^2(\partial D)$ by

$$\mathcal{K}_{D,h}^{(n)}\phi(x) := \int_{\partial D} \mathbb{K}_{h,n}(x, y)\phi(y)d\sigma(y) \quad \forall \phi \in L^2(\partial D) \quad (4.7)$$

for $n \geq 0$. Let Ψ_ε to be the diffeomorphism from ∂D to ∂D_ε given by $\Psi_\varepsilon(x) = x + \varepsilon h(t)\nu(x)$, then we have the following result from [11].

Lemma 4.1. *For $N \in \mathbb{N}$, there exists constant C depending only on N , $\|X\|_{C^2}$ and $\|h\|_{C^1}$ such that the following estimate holds for any $\tilde{\phi} \in L^2(\partial D_\varepsilon)$ and $\phi := \tilde{\phi} \circ \Psi_\varepsilon$,*

$$\left\| \mathcal{K}_{\partial D_\varepsilon}^*[\tilde{\phi}] \circ \Psi_\varepsilon - \mathcal{K}_{\partial D}^*[\phi] - \sum_{n=1}^N \varepsilon^n \mathcal{K}_{D,h}^{(n)}[\phi] \right\|_{L^2(\partial D)} \leq C \varepsilon^{N+1} \|\phi\|_{L^2(\partial D)}. \quad (4.8)$$

From (4.8) we know the shape derivative of the Neumann-Poincaré operator at the variation h and D :

$$[\mathcal{D}(\mathcal{K}_{\partial D}^*)](h) = \mathcal{K}_{D,h}^{(1)}. \quad (4.9)$$

Next we turn our attention to the shape derivatives of the Fredholm eigenvalues. By the Osborn's theorem [29], we have

$$|\lambda_i^\pm(D) - \lambda_i^\pm(D_\varepsilon) - \langle (\mathcal{K}_{\partial D}^* - \mathcal{K}_{\partial D_\varepsilon}^* \circ \Psi_\varepsilon) \phi_i^\pm(D), \phi_i^\pm(D) \rangle| \leq C \|\mathcal{K}_{\partial D}^* - \mathcal{K}_{\partial D_\varepsilon}^* \circ \Psi_\varepsilon\|^2, \quad (4.10)$$

using the facts that $\mathcal{K}_{\partial D_\varepsilon}^*$ is collectively compact, i.e., $\{\mathcal{K}_{\partial D_\varepsilon}^*[\phi] : \|\phi\|_{\mathcal{H}} \leq 1, \varepsilon \geq 0\}$ is sequentially compact, and that $\mathcal{K}_{\partial D_\varepsilon}^* \rightarrow \mathcal{K}_{\partial D}^*$ pointwise. Here $\phi_i^\pm(D)$ are the orthonormal eigenfunctions of the operator $\mathcal{K}_{\partial D}^*$. Now we can easily see from (4.8) and (4.10) the following estimates for the variation of eigenvalues:

$$|\lambda_i^\pm(D) - \lambda_i^\pm(D_\varepsilon) - \varepsilon \langle \mathcal{K}_{D,h}^{(1)} \phi_i^\pm, \phi_i^\pm \rangle| \leq C \varepsilon^2. \quad (4.11)$$

This yields the following result.

Proposition 4.2. *Let λ_i^\pm be simple Fredholm eigenvalues, then their shape derivatives are given by*

$$[\mathcal{D}(\lambda_i^\pm)]_D(h) = \langle \mathcal{K}_{D,h}^{(1)} \phi_i^\pm, \phi_i^\pm \rangle. \quad (4.12)$$

It is worth mentioning that if λ_i is a multiple eigenvalue, it may evolve, under perturbations, into several separated and distinct eigenvalues. The splitting of eigenvalues may only become apparent at high orders in their Taylor expansions with respect to the perturbation parameter. The splitting problem in the evaluation of perturbations in λ_i can be addressed using the arguments in [10, Section 3.4].

5 Optimal shape design using partial spectral data

5.1 Shape design via optimization

In this subsection, we formulate our design problem via an optimization framework. We first recall our shape design problem: given a set of eigenvalues $\{\pm \lambda_i(B)\}_{i=1}^N$ corresponding to a target shape B , we intend to find a shape D such that the eigenvalues of the Neumann-Poincaré operator $\mathcal{K}_{\partial D}^*$, denoted as $\lambda_i(D)$, are approximately equal to $\lambda_i(B)$, i.e., $\lambda_i(D) \approx \lambda_i(B)$ for $1 \leq i \leq N$. In order to achieve this, we have to introduce an appropriate objective functional. In view of the invariance of eigenvalues under rigid transformations and scaling, some effective penalty and regularization terms should be incorporated in the functional to ensure the local existence and uniqueness of the minimizers. This leads us to the following nonlinear functional for our shape design

$$\begin{aligned} \mathcal{J}_{I,\alpha,\beta}(D) &= \frac{1}{2} \sum_{i=1}^I w_i^2 |\lambda_i(D) - \lambda_i(B)|^2 + \frac{\alpha}{2} (|D| - 1)^2 + \frac{\beta}{2} \left(\int_D 2|x_1|^2 + |x_2|^2 \right) \\ &:= (\mathcal{J}_I)_0(D) + \frac{\alpha}{2} \mathcal{A}(D) + \frac{\beta}{2} \mathcal{B}(D), \end{aligned} \quad (5.1)$$

where $I \leq N$ is a given integer index, $\alpha, \beta \in \mathbb{R}^+$ are the parameters for the penalty and the regularization respectively. In view of the large variation of the magnitudes of eigenvalues, we have also introduced some weights w_i in (5.1), which we will naturally choose to be $w_i = 1/\lambda_i(B)$.

For most existing optimization algorithms, we need to compute the variational derivatives of the functionals involved. For this purpose, we introduce some auxiliary tools.

Lemma 5.1. *For a given shape D and $f \in L^1(D)$, the shape derivative of the integral*

$$I(D) := \int_D f dx \quad (5.2)$$

is given by

$$[\mathcal{D}I]|_D(h) = \int_{\partial D} f h dt \quad (5.3)$$

at the variation $h \in \mathcal{C}^1(\partial D)$.

Proof. Given a shape D and $a, b \in \mathbb{R}$ with $a < b$, let $X(t) : [a, b] \rightarrow \partial D$ be an arc-length parametrization of ∂D and $\nu(x)$ be the outward unit normal to ∂D at $x \in \partial D$. For a $h \in \mathcal{C}^1(\partial D)$ which is non-zero everywhere, we consider the ε -perturbation D_ε of D as in (4.2). For sufficiently small $\varepsilon > 0$, we consider a change of variables $(x_1, x_2) \mapsto (\tilde{\varepsilon}, t)$ in an ε -tabular neighborhood of ∂D . Denoting $\det(u, v) = \det \begin{pmatrix} u_1 & v_1 \\ u_2 & v_2 \end{pmatrix}$ for any $u, v \in \mathbb{R}^2$, then we can write

$$\int_{D_\varepsilon} f dx = \int_0^\varepsilon \int_{\partial D} f \det(X' + \tilde{\varepsilon} h \nu', h \nu) dt d\tilde{\varepsilon} + \int_D f dx. \quad (5.4)$$

Using the fact that $X' \perp \nu$ and $\nu' \perp \nu$, we can evaluate the shape derivative of I at h by

$$\begin{aligned} [\mathcal{D}I]|_D(h) &= \left. \frac{\partial}{\partial \varepsilon} \int_{D_\varepsilon} f dx \right|_{\varepsilon=0} \\ &= \int_{\partial D} f \det(X' + \varepsilon h \nu', h \nu) dt|_{\varepsilon=0} \\ &= \int_{\partial D} f \det(X', h \nu) dt \\ &= \int_{\partial D} f h dt. \end{aligned}$$

This leads to the desired formula. □

Using (5.3), we readily know the shape derivative of the following integrals at h :

$$[\mathcal{D}(|D|)](h) = \int_{\partial D} h dt, \quad \left[\mathcal{D} \left(\int_D 2|x_1|^2 + |x_2|^2 dx \right) \right](h) = \int_{\partial D} (2|x_1|^2 + |x_2|^2) h dt. \quad (5.5)$$

With the above preparations we can now discuss the minimization of functional (5.1). In this work we will focus on the Gauss-Newton method for this minimization. We first introduce some more notions.

Given a shape D and $I \in \mathbb{N}$, we write the vector $\lambda_w(D) = (w_1 \lambda_1(D), \dots, w_I \lambda_I(D))^T$ with the superscript T denoting the transpose, and define the Jacobian of the map $D \mapsto \lambda_w(D)$:

$$\begin{aligned} \mathcal{J}_I|_D : L^2(\partial D) &\mapsto \mathbb{R}^I \\ \mathcal{J}_I|_D(h) &= (w_1 [\mathcal{D}\lambda_1]|_D(h), \dots, w_I [\mathcal{D}\lambda_I]|_D(h))^T, \end{aligned} \quad (5.6)$$

where $[\mathcal{D}\lambda_i]|_D(h)$ is the shape derivative of the Fredholm eigenvalue $\lambda_i(D)$ at h , which can be computed by (4.12). Let $\mathcal{J}_I|_D^*$ and $[\mathcal{D}(|D|)]|_D^*$ be the respective $L^2(\partial D)$ adjoint of $\mathcal{J}_I|_D$ and $[\mathcal{D}(|D|)]|_D$, then the Gauss-Newton direction of (5.1) for a shape D can be written as

$$\begin{aligned} N_{I,\alpha,\beta}(D) &:= ([\mathcal{J}_I|_D]^* [\mathcal{J}_I|_D])^{-1} \mathcal{J}_I|_D^* [\lambda_w(D) - \lambda_w(B)] \\ &\quad + \alpha [\mathcal{D}(|D|)]|_D^* (|D| - 1) + \beta \left[\mathcal{D} \left(\int_D 2|x_1|^2 + |x_2|^2 \right) \right]|_D. \end{aligned} \quad (5.7)$$

Now we are ready to formulate the Gauss-Newton method for the minimization of functional (5.1): Let D_n be the n -th approximation of the shape D , and X_n be its arc-length parametrization, then we update X_n by the following iteration:

$$X_{n+1} = X_n - \gamma_n N_{I,\alpha_n,\beta_n}(D_n), \quad (5.8)$$

where γ_n , α_n and β_n are parameters chosen at each iteration and $N_{I,\alpha_n,\beta_n}(D_n)$ is the Gauss-Newton direction as defined in (5.7) with $\alpha = \alpha_n$ and $\beta = \beta_n$. The choice of parameters γ_n , α_n and β_n will be discussed in details in the next subsection.

5.2 Successive refinement for optimization and parameter selection

In this subsection, we describe several detailed strategies for the minimization of the functional $\mathcal{J}_{I,\alpha,\beta}$ in (5.1). These strategies are crucial for our algorithm to work efficiently, and to overcome the difficulties arising from the strong nonlinearity and severe ill-posedness of the current shape design problem.

Our first strategy is a successive refinement technique for the minimization. This strategy is motivated by our observations from numerical experiments. Due to the strong nonlinearity and ill-posedness, iteration (5.8) may stop at some local minima of (5.1) when $I \in \mathbb{N}$ is large. On the other hand, for small I , we observe that iteration (5.8) converges often to a global minimum of (5.1) rapidly even with a poor initial guess. But functional (5.1) does not capture fine features of the target shape if I is too small. These observations motivate us with the following successive refinement strategy: We first minimize $\mathcal{J}_{I,\alpha,\beta}$ in (5.1) with $I = 2$, then minimize $\mathcal{J}_{I,\alpha,\beta}$ for $I = 3, \dots, N$ recursively by using the minimizer of $\mathcal{J}_{I-1,\alpha,\beta}$ as an initial guess. As we will see in our numerical experiments, this strategy works very effectively in avoiding the trapping of the minimization process at some local minima as well as providing us with more fine details for our shape design.

The next strategy is on the choice of parameters α_n and β_n for iteration (5.8). α_n and β_n should be chosen such that the contributions on the search directions in (5.8) from three parts $(\mathcal{J}_I)_0(D)$, $\mathcal{A}(D)$ and $\mathcal{B}(D)$ in (5.1) are balanced at each iteration. Under these considerations, a possible choice is that we first fix two small positive constants C_1 and C_2 , then update α_n and β_n at each iteration by

$$\alpha_n = C_1 \frac{(\mathcal{J}_I)_0(D_n)}{\mathcal{A}(D_n)}, \quad \beta_n = C_1 \frac{(\mathcal{J}_I)_0(D_n)}{\mathcal{B}(D_n)}. \quad (5.9)$$

Our last strategy is on the choice of step size γ_n along the Gauss-Newton direction $N_{I,\alpha_n,\beta_n}(D_n)$, for which we will carry out the line search, namely

$$\gamma_n = \operatorname{argmin} \{ \mathcal{J}_{I,\alpha_n,\beta_n}(X_n - \gamma N_{I,\alpha_n,\beta_n}(D_n)) : \gamma \in \mathbb{R}^+ \}. \quad (5.10)$$

Combining the above three strategies, we arrive at the successive refinement Gauss-Newton shape design algorithm.

Reconstruction Algorithm

Step 1 Given a tolerance ε and an initial guess $D_{1,0}$.

Step 2 For $I = 1$ to N ,

Step 2.1 Set $n := 1$;

Step 2.2 Compute $\alpha_{I,n}$, $\beta_{I,n}$ as in (5.9);

Step 2.3 Compute the Gauss-Newton direction $N_{I,\alpha_n,\beta_n}(D_{I,n})$ as in (5.7);

Find the step size γ_n as in (5.10); Then update $X_{I,n}$ by

$$X_{I,n+1} = X_{I,n} - \gamma_{I,n} N_{I,\alpha_n,\beta_n}(D_{I,n});$$

Step 2.4 If $|\mathcal{J}_{I,\alpha_n,\beta_n}(X_{I,n}) - \mathcal{J}_{I,\alpha_n,\beta_n}(X_{I,n+1})| < \varepsilon$, set $D_{I,\text{stab}} := D_{I,n+1}$; otherwise set $n := n + 1$ and go to **Step 2.2**;

Step 2.5 Take $D_{I+1,0} := D_{I,\text{stab}}$.

Step 3 Find $n_0 \in \{1, 2, \dots, N\}$ such that $D_{n_0,\text{stab}}$ has the minimal residue:

$$(\mathcal{J}_N)_0(D_{n_0,\text{stab}}) = \min_{I \in \{1, 2, \dots, N\}} \{(\mathcal{J}_N)_0(D_{I,\text{stab}})\}.$$

Output $D_{n_0,\text{stab}}$ and stop.

5.3 Numerical results

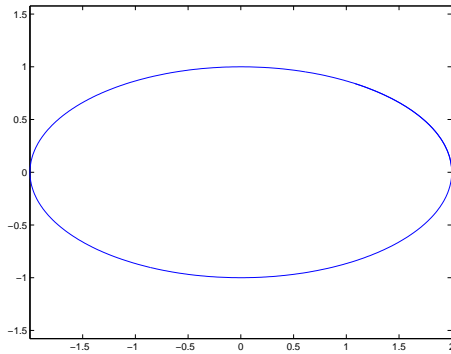
In this section, we shall present several numerical examples to check the performance of the newly proposed reconstruction algorithm in section 5.2 for the optimal shape design using partial spectral data.

Given a domain D , we first obtain the observed data of the forward problem, the Fredholm eigenvalues of D , as in section 3.2. In order to test the robustness of our reconstruction algorithm, we introduce some multiplicative random noise in the eigenvalues of the forward problem as follows:

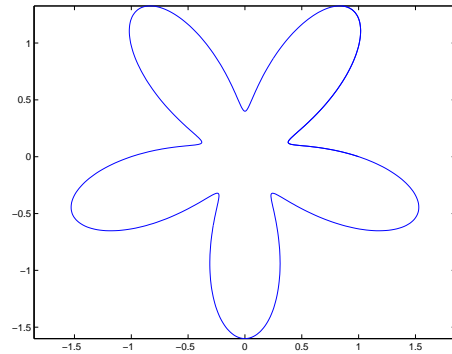
$$\lambda_i^\sigma = \lambda_i(1 + \sigma \xi), \quad i = 1, \dots, N, \quad (5.11)$$

where ξ is uniformly distributed between -1 and 1 and σ corresponds to the level of the noise in the data, which is always set to be 1% in all our examples. It is well-known that the perturbations in the eigenvalues often affect the resulting computations greatly in many applications. It is the same in our current cases. When a new set of random noise is added in the eigenvalues as in (5.11), it gives us a different set of observed data $\{\lambda_i^\sigma\}$. But it is interesting to us that for each example we demonstrate in this section, we obtain only about 2 or 3 basic shapes by our reconstruction algorithm, and all the other shapes obtained with different set of random noise are basically of very small perturbations around these 2 or 3 basic shapes. In our choices of α_n , β_n and tolerance ε , we take $C_1 = C_2 = 0.01$ in (5.9), and $\varepsilon = 5 \times 10^{-4}$. And we will take the first 7 eigenvalues in the observed data, namely $N = 7$ in our reconstructions.

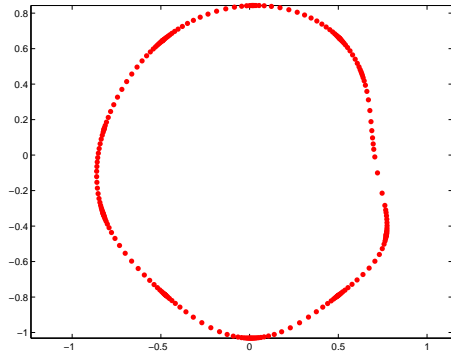
Example 1. This example tests an ellipse of the form (3.19) as the target shape; see Figure 3(a). Figures 3(c) and 3(d) show two reconstructed shapes that appear most frequently with different sets of random noise. The initial guess in the reconstruction is a shape of the form (3.20) with $\delta = 0.6$, $m = 5$; see Figure 3(b). Clearly this is a very poor initial shape, but the reconstructed shapes seem quite satisfactory.



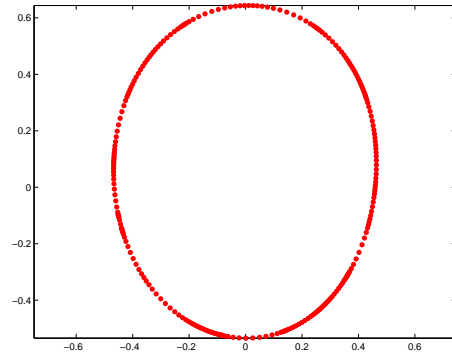
(a)



(b)



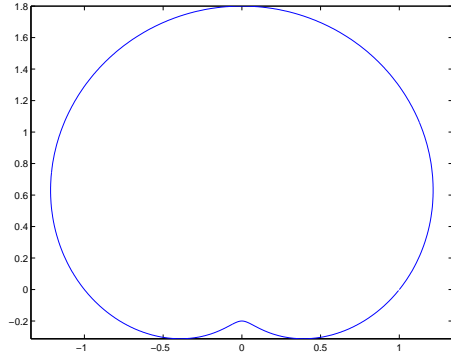
(c)



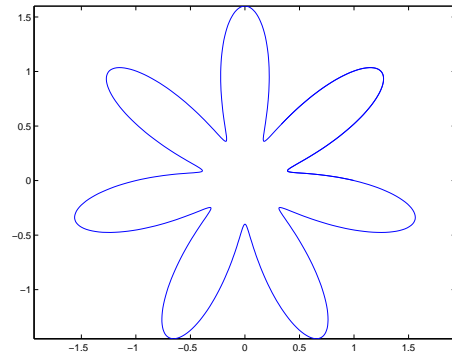
(d)

Figure 3: (a): target shape in Example 1; (b): initial guess; (c) and (d): two reconstructed shapes that appear most frequently with 1% random noise.

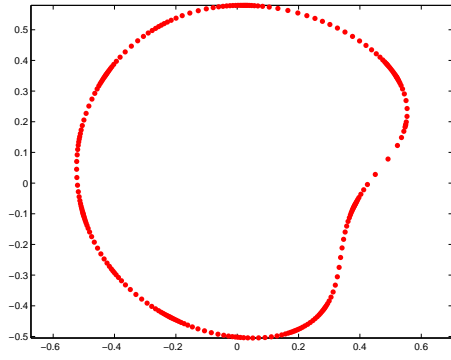
Example 2. In this example, our target shape is a heart-shaped domain of the form (3.20) with $\delta = 0.8$, $m = 1$; see Figure 4(a). Starting with a very poor initial guess, a shape of the form (3.20) with $\delta = 0.6$, $m = 7$ (see Figure 4(b)), two reconstructed shapes that appear most frequently with different sets of random noise are shown in Figures 4(c) and 4(d). Considering the invariance of the target shape up to translation, rotation, and scaling, our reconstructions seem to be rather satisfactory.



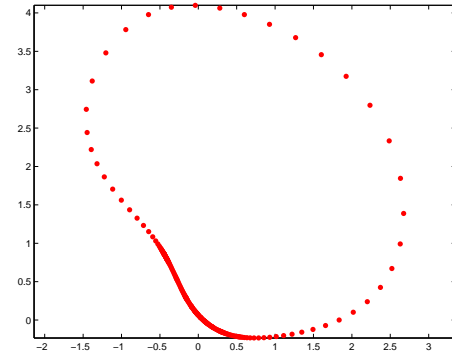
(a)



(b)



(c)



(d)

Figure 4: (a): target shape in Example 2; (b): initial guess; (c) and (d): two reconstructed shapes that appear most frequently with 1% random noise.

Example 3. A peanut-shaped domain of the form (3.20) with $\delta = 0.6$, $m = 2$ is investigated in this example; see Figure 5(a). Our initial guess is of the form (3.20) with $\delta = 0.6$, $m = 5$; see Figure 5(b). Figure 5 (c) and Figure 5(d) present two reconstructed shapes that appear most frequently with different sets of random noise.

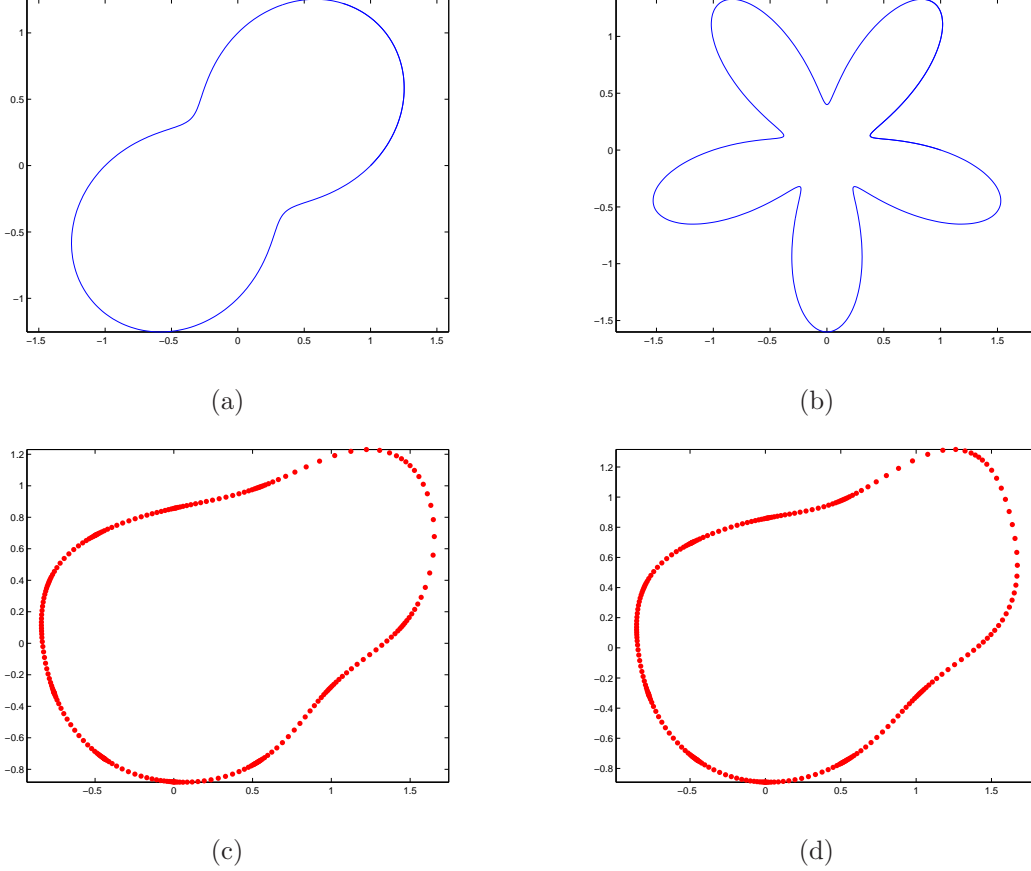


Figure 5: (a): target shape in Example 3; (b): initial guess; (c) and (d): two reconstructed shapes that appear most frequently with 1% random noise.

Example 4. In this example, we consider a pear-shaped domain of the form (3.20) with $\delta = 0.3$, $m = 3$; see Figure 6(a). We start from the initial guess of the form (3.20) with $\delta = 0.6$, $m = 3$; see Figure 6(b). The reconstructed shapes that appear most frequently from the data polluted by different sets of random noise are shown in Figure 6(c) and Figure 6(d). Considering the random noise added in the spectral data and the sensitivity of eigenvalue problem, our reconstructions prove to be quite satisfactory.

6 Concluding remarks

In this work we have proposed numerical methods to recover the Fredholm eigenvalues of a domain from the measurements of its polarization tensor at multiple contrasts or frequencies. Then we have developed an optimal shape design algorithm (up to rigid transformations and scaling) based on partial knowledge of Fredholm eigenvalues. Both inverse problems are highly nonlinear and severely ill-posed, but our numerical experiments have demonstrated the effectiveness and robustness of the proposed reconstruction algorithms. By using only the first few Fredholm eigenvalues, we have regularized the considered inverse problems. We expect that our results will have important applications in plasmon resonant nanoparticle design and in multifrequency imaging and classification of small anomalies from electrical capacitance measurements.

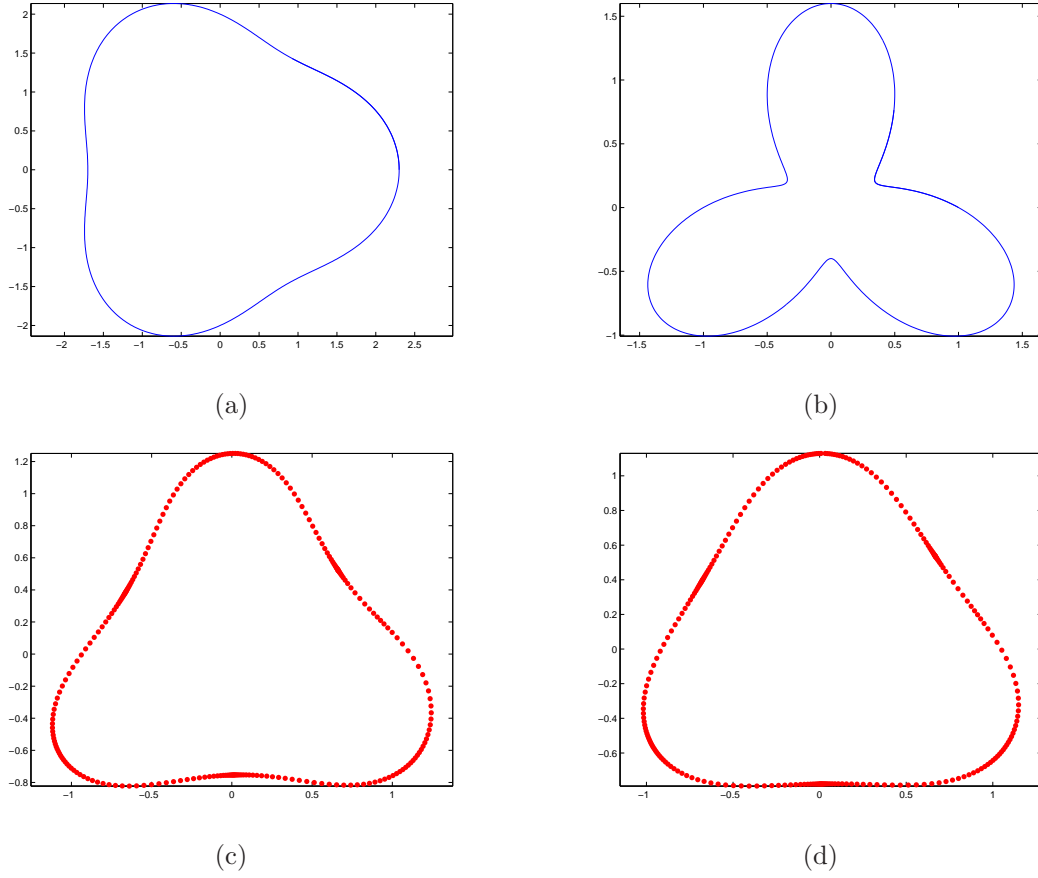


Figure 6: (a): target shape in Example 4; (b): initial guess; (c) and (d): two reconstructed shapes that appear most frequently with 1% random noise.

A Pulse shape design

In this section, we show how to acquire the PT at multiple contrasts in electrical capacitance tomography using pulsed imaging.

Given a harmonic function u_0 in \mathbb{R}^d , a final time $T > 0$, and pulse shape $h(t)$, that is supposed to be a compactly supported function in $(0, T)$, electrical capacitance tomography is to reconstruct the inclusion D from measurements of the solution $u(x, t)$ to the following system

$$\begin{cases} \nabla \cdot (\varepsilon_D + \varepsilon'_c \partial_t) \nabla u = 0 & \text{in } \mathbb{R}^d \times (0, T), \\ u(x, t) - u_0(x)h(t) = O(|x|^{1-d}) & \text{as } |x| \rightarrow \infty, \text{ for all } t \in (0, T), \end{cases} \quad (\text{A.1})$$

where ε'_c is a positive constant. Here, ε_c and ε'_c are respectively the conductivity and permittivity of D . The background medium $\mathbb{R}^d \setminus \overline{D}$ is assumed to be with conductivity ε_m and 0 permittivity. In the time-harmonic regime, we call $\varepsilon_c + i\omega\varepsilon'_c$ the admittivity of D with ω being the operating frequency.

Let $\sigma := \varepsilon_c/\varepsilon_m$ and $\varepsilon := \varepsilon'_c/\varepsilon_m$. According to [9], we can reconstruct the polarization tensor $M(\lambda(t), D)$ from the measurements of u for x being far away from D , where

$$\lambda(t) = \frac{(\sigma + 1)h(t) + \varepsilon h'(t)}{2(\sigma - 1)h(t) + 2\varepsilon h'(t)}, \quad t \in (0, T). \quad (\text{A.2})$$

From the above formula, we can see that a different pulse h gives a different curve $\gamma := \{\lambda(t) \in \mathbb{C} : t \in (0, T)\}$ on the complex plane \mathbb{C} . Motivated from Section 3, we aim to find a pulse $h \in \mathcal{C}_c^\infty(0, T)$ for some $T > 0$ such that the curve $\gamma := \{\lambda(t) \in \mathbb{C} : t \in (0, T)\}$ given by (A.2) encloses the spectrum of $\sigma(\mathcal{K}_{\partial D}^*) \subset (-1/2, 1/2]$.

Therefore, we shall investigate different possible shapes of the impulse h which gives an optimal shape of the curve γ . Our desired γ should be a smooth simple closed curve enclosing $(-0.5, 0.5]$. Then we can recover the eigenvalues of $\sigma(\mathcal{K}_{\partial D}^*)$ from $M(\lambda, \partial D)$ as in subsection 3.1.

By explicit calculations, if we let

$$p = \frac{(\sigma + 1) - 2(\sigma - 1)\lambda}{\varepsilon(1 - 2\lambda)}, \quad (\text{A.3})$$

then we have from (A.2) the following explicit form for the pulse h :

$$h(t) = C \exp\left(\int_0^t p(s) ds\right), \quad (\text{A.4})$$

where C is a constant. Letting $\lambda = Ae^{2\pi it}$, we get

$$h(t) = e^{-2t}(2Ae^{2\pi it} - 1)^{-\frac{i}{2\pi}}, \quad (\text{A.5})$$

where the function z^i is defined as $z^i := e^{i \log z}$. Note that although the solution in (A.5) is not necessarily compactly supported, we can always extend the function to a compactly supported smooth function on $(-\varepsilon, T + \varepsilon)$ for some $\varepsilon > 0$.

Given parameters $\sigma = 3$, $\varepsilon = 2$ and $T = 20$, we have tried different shapes of the pulse $h(s)$.

Example 1 In this example we choose $h(t) = A(t)\phi(t)$, where $\phi(t) = \exp(\frac{(t-a)\pi}{2\sigma_0}i + \frac{\pi}{2}i)$ and $A(t) = \frac{1}{\sqrt{2\pi\sigma_0}} \exp\left(-\frac{(t-a)^2}{2\sigma_0^2}\right)$ with $\sigma_0 = 0.3, a = 3$. The real part of the curve $h(t)$ and its corresponding curve $\lambda(t)$ on the complex plane \mathbb{C} according to (A.2) are shown in Figure 7.

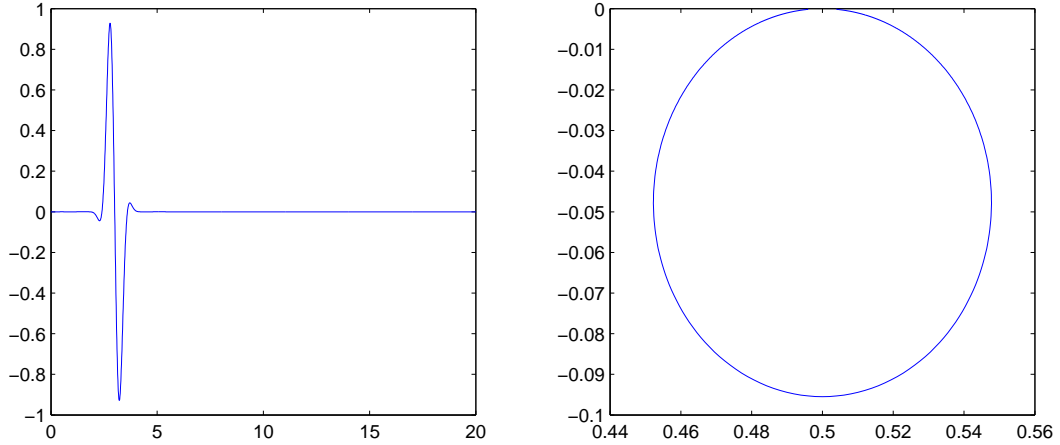


Figure 7: Real part of impulse $h(t)$ in Example 1 (left); Curve $\lambda(t)$ according to (A.2) (right).

Example 2 Choose $h = -A(t)\phi(t)$, where $\phi(t) = \exp(i \cos(t - a)\pi)$ and $A(t) = \frac{1}{\sqrt{2\pi\sigma_0}} \exp\left(-\frac{(t-a)^2}{2\sigma_0^2}\right)$ with $\sigma_0 = 0.3, a = 3$. Figure 8 shows the real part of the curve $h(t)$ and its corresponding curve $\lambda(t)$ according to (A.2).

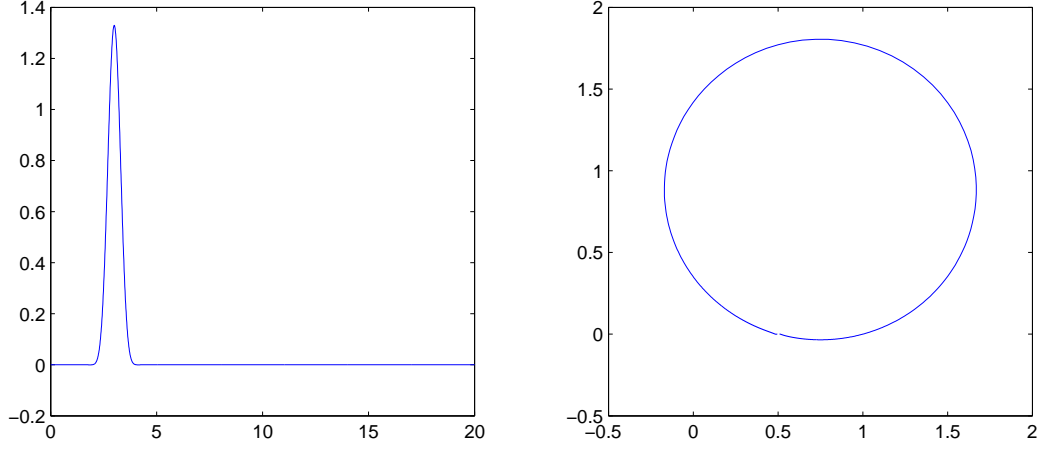


Figure 8: Real part of impulse $h(t)$ in Example 2 (left); Curve $\lambda(t)$ according to (A.2) (right).

Example 3 We choose $h = e^{-2t}(2Ae^{2\pi it} - 1)^{-\frac{i}{2\pi}}$. The real part of the curve $h(t)$ and its corresponding curve $\lambda(t)$ according to (A.2) is shown on Figure 9.

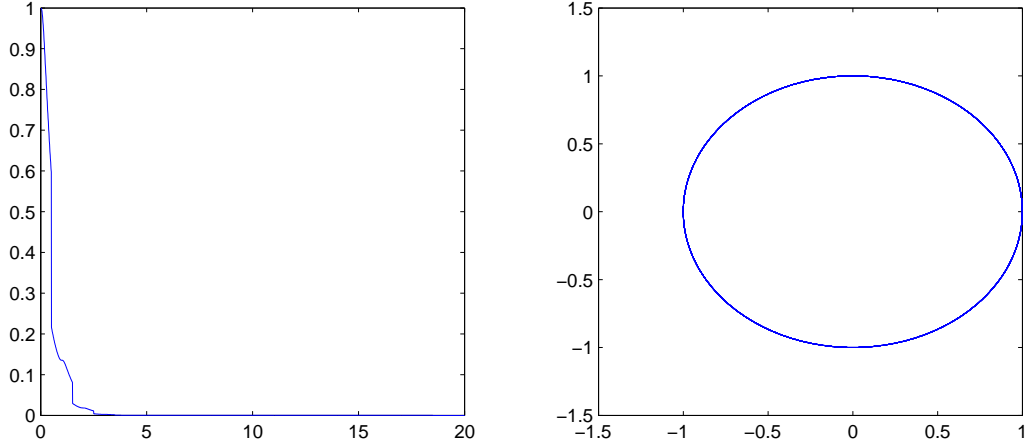


Figure 9: Real part of impulse $h(t)$ in Example 3 (left); Curve $\lambda(t)$ according to (A.2) (right).

B Multiply connected objects

In this section, we briefly investigate the eigenvalue of the Neumann-Poincaré operator of a domain consisting of two identical copies of a non-overlapping shape with the same contrast. Let the shape D_1 be given, we consider the shape

$$D_v := D_1 \cup D_2, \quad (\text{B.1})$$

where $D_2 := D_1 + v$ and $v \in \mathbb{R}^2$ is such that the distance $d(D_1, D_2)$ between D_1 and D_2 is positive. The Neumann-Poincaré operator $\mathbb{K}_{\partial D_v}^*$ associated with D_v is given by [6]

$$\mathbb{K}_{\partial D_v}^* := \begin{pmatrix} \mathcal{K}_{\partial D_1}^* & \frac{\partial}{\partial \nu_1} \mathcal{S}_{\partial D_2} \\ \frac{\partial}{\partial \nu_2} \mathcal{S}_{\partial D_1} & \mathcal{K}_{\partial D_2}^* \end{pmatrix}. \quad (\text{B.2})$$

We are interested in how the eigenvalues of $\mathbb{K}_{\partial D_v}^*$ behave as v varies, and particularly when $d(D_1, D_2) \rightarrow 0$. As an example, we consider an ellipse, D_1 , of the form (3.19).

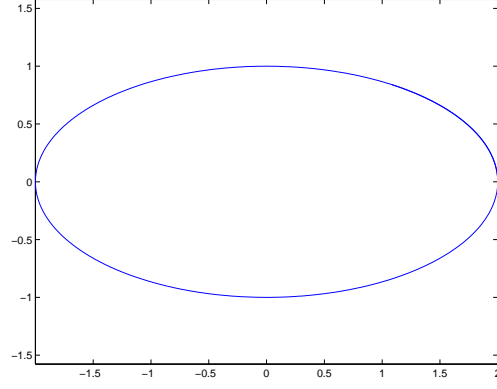
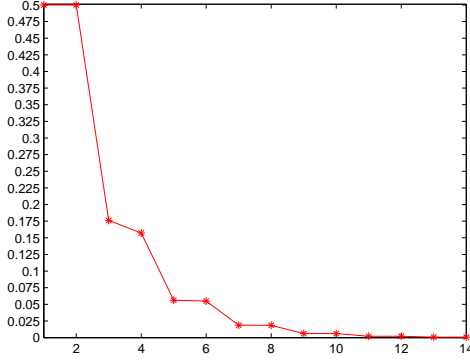
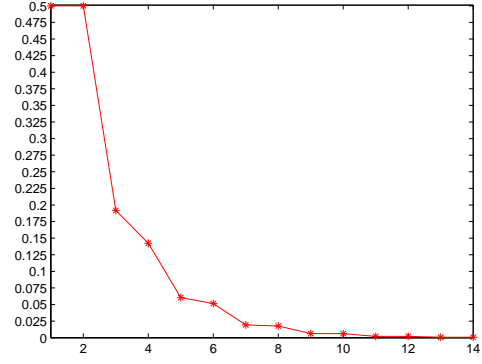


Figure 10: The ellipse D_1 .

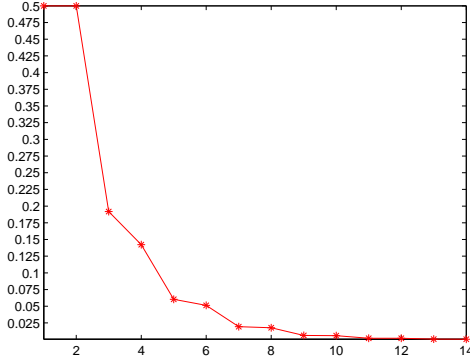
Letting $v = (2^k + 2)(0, 1)$ where $k = 5 - n$ and $n = 1, 2, \dots, 10$, we observe the change of the spectrum of $\mathbb{K}_{\partial D_v}^*$. Figure 11 shows the eigenvalues of $\mathbb{K}_{\partial D_v}^*$ which is larger than 0.0005 as v varies.



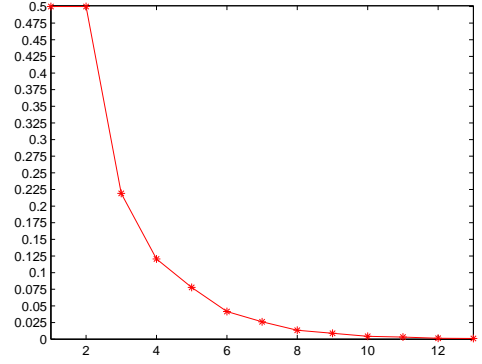
(a)



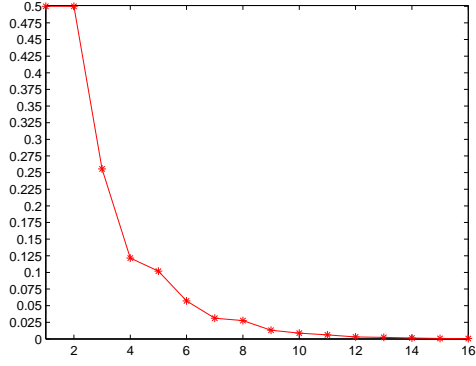
(b)



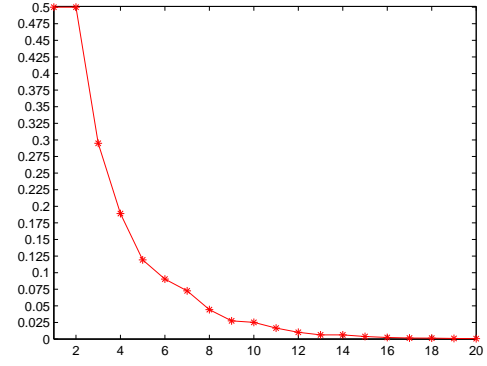
(c)



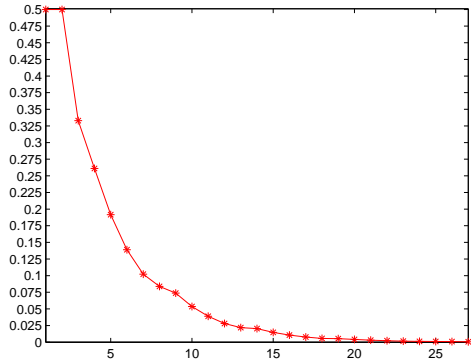
(d)



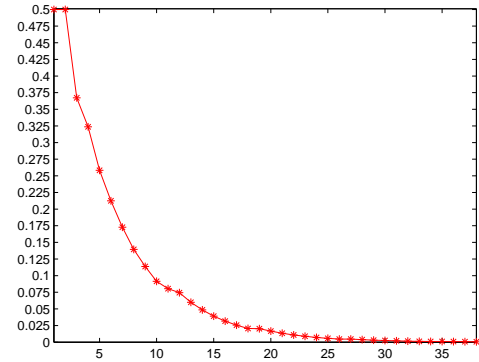
(e)



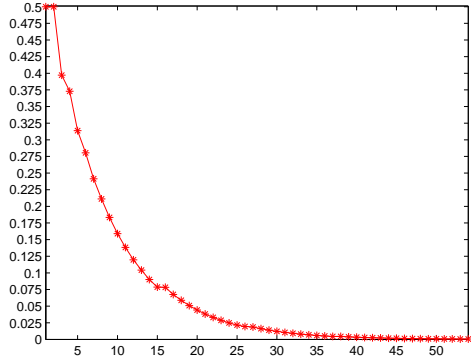
(f)



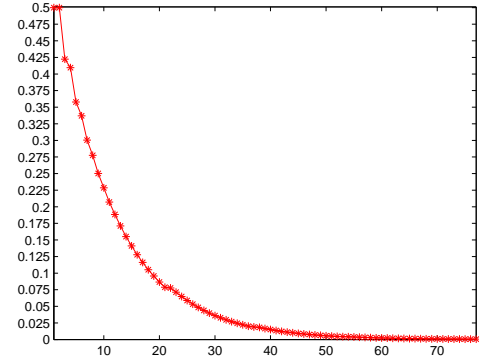
(g)



(h)



(i)



(j)

Figure 11: Spectrum of $\mathbb{K}_{\partial D_v}^*$ in (B.2) as $k = 5 - n$ with $n = 1, 2, \dots, 10$, starting from (a) with $n = 1$ to (j) with $n = 10$.

We note that the spectrum converges to a smoother curve where there are fewer “steps”. Moreover, the multiplicity of the eigenvalue $1/2$ reflects the number of connected components of D_v ; see [6, 13].

References

- [1] L.V. Ahlfors, Remarks on the Neumann-Poincaré integral equation, Pacific J. Math., 3 (1952), 271–280.

- [2] H. Ammari, T. Boulier, and J. Garnier, Modeling active electrolocation in weakly electric fish, *SIAM J. Imaging Sci.*, 5 (2013), 285–321.
- [3] H. Ammari, T. Boulier, J. Garnier, W. Jing, H. Kang, and H. Wang, Target identification using dictionary matching of generalized polarization tensors, *Found. Comput. Math.*, DOI: 10.1007/s10208-013-9168-6.
- [4] H. Ammari, T. Boulier, J. Garnier, and H. Wang, Shape identification and classification in electrolocation, *arXiv:1302.6384*.
- [5] H. Ammari, G. Ciraolo, H. Kang, H. Lee, and G.W. Milton, Spectral theory of a Neumann-Poincaré-type operator and analysis of cloaking due to anomalous localized resonance, *Arch. Ration. Mech. Anal.*, 208 (2013), 667–692.
- [6] H. Ammari, G. Ciraolo, H. Kang, H. Lee, and K. Yun, Spectral analysis of the Neumann-Poincaré operator and characterization of the stress concentration in anti-plane elasticity, *Arch. Ration. Mech. Anal.*, 208 (2013), 275–304.
- [7] H. Ammari, J. Garnier, W. Jing, H. Kang, M. Lim, K. Solna, and H. Wang, *Mathematical and Statistical Methods for Multistatic Imaging*, Lecture Notes in Mathematics 2098, Springer-Verlag, Berlin, 2013.
- [8] H. Ammari, J. Garnier, H. Kang, M. Lim, and S. Yu, Generalized polarization tensors for shape description, *Numer. Math.*, DOI 10.1007/s00211-013-0561-5.
- [9] H. Ammari and H. Kang, *Polarization and Moment Tensors: With Applications to Inverse Problems and Effective Medium Theory*, Applied Mathematical Sciences 162, Springer-Verlag, New York, 2007.
- [10] H. Ammari, H. Kang, and H. Lee, *Layer Potential Techniques in Spectral Analysis*, Mathematical Surveys and Monographs series 153, Amer. Math. Soc., Rhode Island, 2009.
- [11] H. Ammari, H. Kang, M. Lim, and H. Zribi, The generalized polarization tensors for resolved imaging. Part I: Shape reconstruction of a conductivity inclusion, *Math. Comp.*, 81 (2012), 367–386.
- [12] R.D. Benguria, H. Linde, and B. Loewe, Isoperimetric inequalities for eigenvalues of the Laplacian and the Schrödinger operator, *Bull. Math. Sci.*, 2 (2012), 1–56.
- [13] E. Bonnetier and F. Triki, Pointwise bounds on the gradient and the spectrum of the Neumann-Poincaré operator: the case of 2 discs, *Multi-scale and high-contrast PDE: from modelling, to mathematical analysis, to inversion*, 81–91, *Contemp. Math.*, 577, Amer. Math. Soc., Providence, RI, 2012.
- [14] E. Bonnetier and F. Triki, On the spectrum of the Poincaré variational problem for two close-to-touching inclusions in 2D, *Arch. Ration. Mech. Anal.*, 209 (2013), 541–567.
- [15] J. Flusser, T. Suk, B. Zitov, and I. Ebrary, *Moments and moment invariants in pattern recognition*, Wiley Online Library, 2009.
- [16] D. Grieser, The plasmonic eigenvalue problem, *arXiv:1208.3120*.
- [17] J. Helsing and K/M. Perfekt, On the polarizability and capacitance of the cube, *Appl. Comp. Harmonic Anal.*, 34 (2013), 445–468.
- [18] C. D. Hopkins and G. W. M. Westby, Time domain processing of electrical organ discharge waveforms by pulse-type electric fish, *Brain Behav. Evol.*, 29 (1986), 77–104.
- [19] M.K. Hu, Visual pattern recognition by moment invariants, *Trans. Inform. Theor.*, 8 (1962), 179–187.

- [20] P.K. Jain, K.S. Lee, I.H. El-Sayed, and M.A. El-Sayed, Calculated absorption and scattering properties of gold nanoparticles of different size, shape, and composition: Applications in biomedical imaging and biomedicine, *J. Phys. Chem. B*, 110 (2006), 7238–7248.
- [21] S.X. Liao and M. Pawlak, On image analysis by moments, *IEEE Trans. Pattern Anal. Mach. Intellig.*, 18 (1996), 254–266.
- [22] H. Kang and J.K. Seo, Inverse conductivity problem with one measurement: uniqueness of balls in \mathbb{R}^3 , *SIAM J. Appl. Math.*, 59 (1999), 851–867.
- [23] O.D. Kellogg, *Foundations of Potential Theory*, Reprint from the first edition of 1929. Die Grundlehren der Mathematischen Wissenschaften, Band 31 Springer-Verlag, Berlin-New York, 1967.
- [24] D. Khavinson, M. Putinar, and H.S. Shapiro, Poincaré’s variational problem in potential theory, *Arch. Rational Mech. Anal.*, 185 (2007) 143–184.
- [25] S. Kim, J. Lee, J.K. Seo, E.J. Woo, and H. Zribi, Multifrequency trans-admittance scanner: mathematical framework and feasibility, *SIAM J. Appl. Math.*, 69 (2008), 22–36.
- [26] T. Kotnik, D. Miklavcic, and T. Slivnik, Time course of transmembrane voltage induced by time-varying electric fields-a method for theoretical analysis and its application, *Bioelectrochemistry and Bioenergetics*, 45 (1998), 3–16.
- [27] I.D. Mayergoyz, D.R. Fredkin, and Z. Zhang, Electrostatic (plasmon) resonances in nanoparticles, *Phys. Rev. B*, 72 (2005), 155412.
- [28] I.D. Mayergoyz and Z. Zhang, Numerical analysis of plasmon resonances in nanoparticles, *IEEE Trans. Mag.*, 42 (2006), 759–762.
- [29] J.E. Osborn, Spectral approximation for compact operators, *Math. Comp.*, 29 (1975), 712–725.
- [30] D. Sarid and W.A. Challener, *Modern Introduction to Surface Plasmons: Theory, Mathematical Modeling, and Applications*, Cambridge University Press, New York, 2010.
- [31] M. Schiffer, The Fredholm eigen values of plane domains, *Pacific J. Math.*, 7 (1957), 1187–1225.
- [32] M. Schiffer and G. Schober, An extremal problem for the Fredholm eigenvalues, *Arch. Rational Mech. Anal.*, 44 (1971/72), 83–92.
- [33] J.K. Seo and E.J. Woo, Multi-frequency electrical impedance tomography and magnetic resonance electrical impedance tomography, *Mathematical modeling in biomedical imaging I*, 1–71, Lecture Notes in Mathematics 1983, Springer-Verlag, Berlin, 2009.
- [34] G. Springer, Fredholm eigenvalues and quasiconformal mapping, *Acta Math.*, 111 (1964), 121–142.